Structural analysis of DEMO divertor cassette body and design study based on RCC-MRx

Paolo Frosi[a,*], Christian Bachmann[b], Giuseppe Di Gironimo[c], Giuseppe Mazzone[a], Domenico Marzullo[c], Jeong-Ha You[d]

[a] Department of Fusion and Technology for Nuclear Safety and Security, ENEA C. R. Frascati, via E. Fermi 45, 00044 Frascati, Roma, Italy
[b] EUROfusion, PPPT, Boltzmann Str. 2, 85748 Garching, Germany
[c] CREATE Consortium/University of Naples Federico II, Department of Industrial Engineering (DII), Piazzale Tecchio 80-80125 Napoli, Italy
[d] Max Planck Institute for Plasma Physics, Boltzmann Str. 2, 85748 Garching, Germany

HIGHLIGHTS

- The last geometrical conception of the DEMO Divertor Cassette has been considered and the initial finite element model has been improved to obtain mapped mesh. The loads that really act on this component have been evaluated but at this stage of the analysis they have been applied as uniformly distributed because the values havent been supplied in a table-formatted manner. In spite of this simplification, the obtained results allow some useful deductions: the main role played by the thermal loads has been confirmed, and moreover the electric-magnetic loads (due to halo and eddy current) have been numerically obtained from the real DEMO Divertor geometry: they have been applied with the same uniform distribution and it seems that their action isnt really negligible.
- Another simplified 2D fem model has been obtained and it supplies stress results that have the same order of magnitude of the aforementioned 3D model.
- An early application of RCC-MRx design rule have also been considered:the component seems to be safe at least in nominal conditions.

ARTICLE INFO

Keywords:
FEM
DEMO
Divertor
Structural analysis
Thermal analysis
RCC-MRx

ABSTRACT

This paper refers to the activity of structural design of DEMO Divertor in the framework of the EUROfusion Consortium. The structural analysis and its preparatory assessments were carried on since a year and the first results were published in a previous paper. The Cassette Body has been examined considering the most conservatives loads (e.g. coolant pressure, volumetric nuclear heating and electro-magnetic loads) according to their latest estimates. This work is based on the design-by-analysis approach adopted in the conceptual design phase of the DEMO Divertor. This design activity has been focused on some key parameters e.g. loads, main geometric dimensions, positions of the Cassette attachments on the vacuum vessel, way of loads application to characterize the structural behavior of the Divertor Cassette. In addition to the existing 3D solid element model, a shell element model has also been developed: with this new model a parametric analysis can be done for a fast optimization. The structural assessment was done according to the Design and Construction Rules for Mechanical Components of Nuclear Installation (RCC-MRx).

1. Introduction

The present paper reports the latest progress in the structural design activity of the European DEMO Divertor Cassette Body which has been conducted in the framework of the work package “Divertor” of the EUROfusion Consortium [1–5]. The present structural design includes computational analysis and code-based assessment criteria. For this investigation the physical loads, that determine mainly the mechanical behavior of the divertor, must be taken into account. The thermal load from plasma that is nuclear (neutronic and photonic) heating, the static load due to coolant pressure (and the related reaction forces on the supports) and the dynamic load due to electromagnetic forces have been considered. The structural analysis is anticipated by

* Corresponding author.

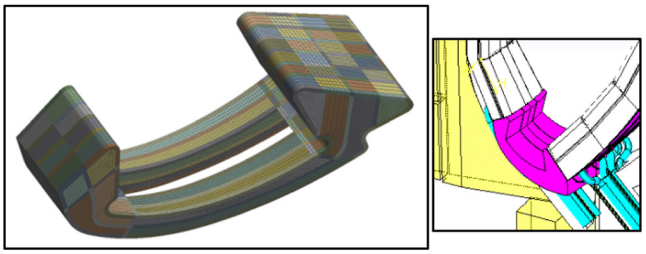

Fig. 1. Mapped mesh of Cassette Divertor and detail of its position.

preparatory investigations for loads evaluation and followed by structural design assessment in which the computed stress intensities are used as input values in the design criteria. In order to obtain reliable results, the finite element models have been optimized trying different element type and meshing strategy. The position and the function of the supports have also been optimized with a trial-and-error process. As design rules, the criteria formulated in the French code RCC-MRx have been preliminary employed in this study [6]. Aside from a model adopting the conventional 3D brick elements, an alternative parametric model using shell element is employed. Some implications related to a future design optimization are discussed.

2. Geometry model and meshing

The present campaign of analyses represents an improvement of the previous calculations [1]. The main differences and results are going to be explained in the following.

The most important enhancement produced in the whole analysis has regarded the mesh: the solid model that was initially made up of only one volume has been divided in several connected parts to obtain the more confident mapped mesh as it can be seen in Fig. 1.

This action has been considered a priority for the progression of the study to give more overall reliability to the analysis. As usual, some preliminary attempts have been executed to choose a suitable element size. Finally a global size of 25 mm has been adopted and the model results with 71,813 (linear) elements and 376,473 nodes.

As reported in [1], it has been established that the Cassette is made of Eurofer whose physical properties can be found in [6]. All the choices related to material modeling can be found in [1] and here they have been still adopted.

3. Thermal loads, boundary conditions and thermal analysis

The initial step of the study has regarded the thermal analysis: it essentially deals with volumetric nuclear power density and convective cooling. The first load value has been obtained from [7] where a detailed evaluation of the nuclear heating has been summarized. With very easy calculations from [7] the volumetric nuclear power density ($2.4737 \cdot 10^6$ W/m^3) has been obtained and then declared inside the model. But in doing so the nuclear heating has been applied uniformly: instead, as reported in [7], in reality the higher values are distributed in the inboard region and lower values in the outboard region; but this accurate distribution has not been possible to apply on the model.

The values related to convective cooling are: the convection film coefficient equals to 10 kW/(m^2 K) like stated in [1] and the water bulk temperature equals to 210 °C (the outlet value has been chosen in order to be conservative) according the last agreements of the Balance of Plant (BoP) that are not published yet. All the internal surfaces (reported in Fig. 2) that are interested by convective and pressure loads have been clearly identified beforehand for the

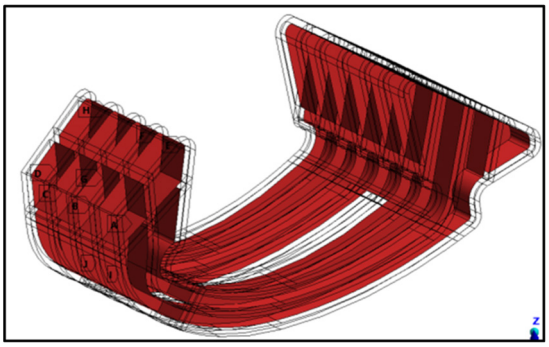

Fig. 2. Internal surfaces for application of thermal and mechanical loads.

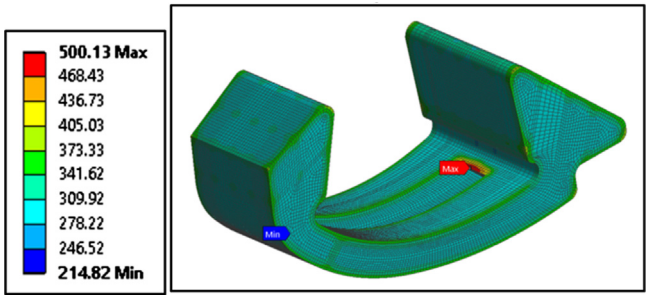

Fig. 3. Contour plot of temperature (°C).

whole set of the following analysis. This is a steady state analysis: so besides the balance of inlet (nuclear heating) and outlet (convective cooling) thermal power, no thermal boundary conditions have been defined and the component has been considered adiabatic.

In doing so, the temperature distribution has been evaluated and it can be seen in Fig. 3.

The peak value of temperature related to the sharp corners can be surely neglected because they can be weakened with a detailed dimensioning of the chamfers; the value of 309.92 °C corresponding to the end of the third step in the legend can be chosen as representative of the state of the cassette and it is not a dangerous level although the aforementioned uniform application of thermal loads. The creep temperature limit is 375 °C [6] and, with the previous hypothesis, this phenomenon can be neglected. More, the thermal gradient inside the component and the following stresses arising from differential thermal expansion have been neglected. Nevertheless it must be kept in mind that it has been dealt with a steady state analysis that is not far from the real situation in which the pulses are foreseen to last for several minutes: so the duration of the pulse turns in favour of a softening of these thermal gradients. In any case this point shall be engaged in a future work.

4. Structural loads, boundary conditions and structural analysis

The following step has regarded the structural analysis. The temperature distribution and the water pressure (whose value of 3.5 MPa comes from the same BoP mentioned above) have been applied with the definition of the elastic-plastic kinematic hardening material model as in [1].

The resulting Von Mises stresses have been reported in Fig. 4. These values are too high only at inwards corners that might be avoided with a detailed design of the sharp regions. It is not possible to define a single maximal admissible temperature because the yielding and the ultimate stresses depend on it. So the overall information that the component is far from the previous limits, can

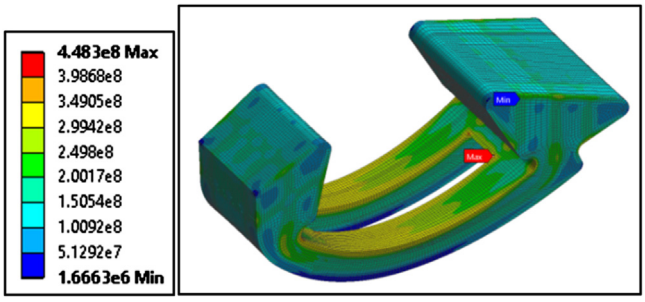

Fig. 4. Equivalent stress for thermal and mechanical loads (Pa).

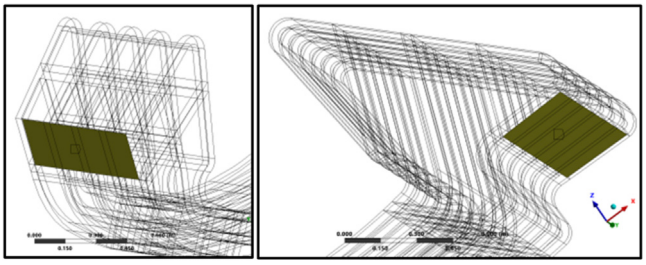

Fig. 5. Inboard (left) and outboard (right) position of the attachments.

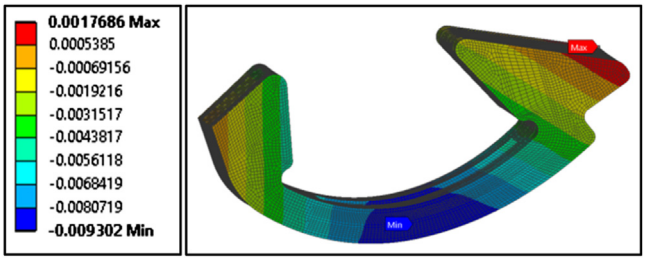

Fig. 6. Vertical displacements of cassette (m).

be obtained from the plastic strain contour plot that is always zero (not reported).

It is worth to be mentioned the study (executed before obtaining any valuable results of the structural simulations) about the position of the attachments. The central, the intermediate and lateral regions have been chosen to perform some tests with different constraints (radial, toroidal and vertical displacements nullified by turns), in a symmetric and asymmetrical position. The solution that exhibits the lowest values of stress has been chosen and the related positions of the attachments are reported in Fig. 5.

The physical constraints that have been simulated are: radial, toroidal and vertical displacements nullified, then the rotations about radial and vertical axis have been nullified and finally the rotations about the toroidal direction have been kept free. This physical condition has been mathematically implemented using the Ansys tool named *remote point*: that is the above mentioned conditions on displacements and rotations have been declared on the centroids of the surfaces reported in Fig. 5; in doing so these centroids act as *remote points*. This choice is seemed to be wise: in Fig. 6 the vertical displacements have been reported and it can be seen that the cassette is subjected to a flexural action that increases the curvature in its central region that is the most slender zone. So a certain quantity of strain energy has been stored in a slender zone and it keeps the stress values reasonably low.

But this result shall be reviewed because of the aforementioned uniform action of the nuclear heating: this distribution is expected to exercise a high flexural action that should straighten the

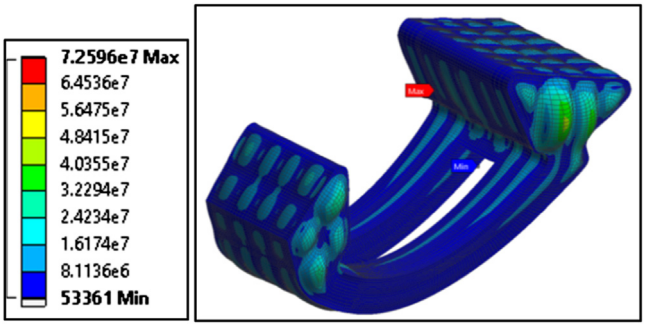

Fig. 7. Equivalent stresses due to water pressure (Pa).

Table 1
Resultant forces (MN) and resultant moments (MNm) due to an heuristic case of halo currents.

F_{rad}	F_{tor}	F_{ver}	M_{rad}	M_{tor}	M_{ver}
2.72	0	5.70	0	45.4	0

curvature of the cassette and it should result in an important action on the attachments that can't be highlighted now.

The Fig. 7 reports the Von Mises stresses related to the water pressure acting alone: it produces a very low level of stresses as already found in [1]: this result shows that the stress distribution of Fig. 4 is mainly due to thermal loads that finally result high (on average) in spite of the simplification given by the uniformity of their application.

This fact that the stresses reported in Fig. 4 are almost completely due to the thermal loads is confirmed by the case with thermal loads acting alone: here the Von Mises stresses (not reported) are almost equal to those ones in Fig. 4. Moreover it is worth to mention that the maximum value in Fig. 7 has been obtained in an inwards corner of the internal cooling volumes and other peak values can be found in similar regions: so once again a detailed design is required to avoid these singularities.

5. EM loads and off-design structural analysis

Another chapter of this study has regarded the influence of disruption events on this tokamak component. The first case is related to the study reported in [8], really related to Demo Divertor, in which the contribution of the halo currents to the electro-magnetic forces has been evaluated. A forward step respect to [1] has been done: it is no more necessary to adopt the ITER values, excluding any problem of translation and adaptation of those results; but also here it has not been possible to manage the real distribution of those forces: so the resultants (forces and moments) had to be divided uniformly on all nodes. The centroid of the cassette has been chosen as *remote point* and the lateral vertical surfaces have been associated to it to *spread* the resulting moments. The most severe case studied in [8] has been used and it is reported in Table 1.

In Fig. 8 there are the resulting Von Mises stresses related to this case.

The stress level is higher than that reported in Fig. 4, and the plastic strains regard a zone a bit enlarged (not reported). Some refinements seem necessary according this case.

Another case of disruption has been taken from the most severe case reported in [9] with the same assumption of uniform distribution of resultant forces and moments. The case extracted from this study has regarded the time at the end of the current quench. The values considered in this situation are reported in Table 2.

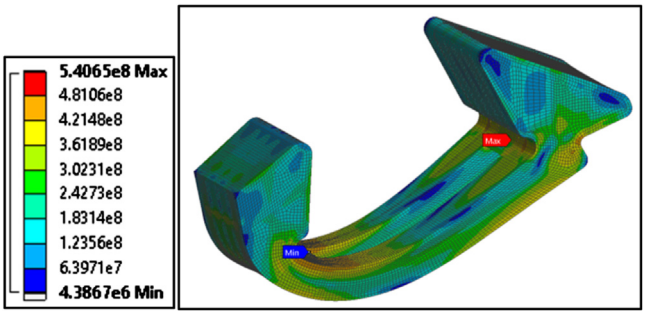

Fig. 8. Equivalent stresses due to halo currents (Pa).

Table 2
Resultant forces (MN) and resultant moments (MNm) due to an heuristic case of eddy and halo currents.

F_{rad}	F_{tor}	F_{ver}	M_{rad}	M_{tor}	M_{ver}
0.32	0.7	1	1.3	0.29	5.1

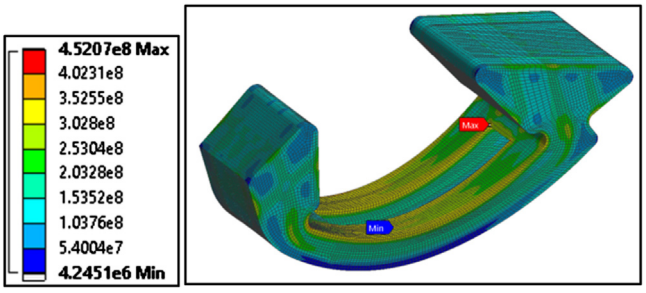

Fig. 9. Equivalent stresses due to eddy and halo currents (Pa).

Now the state of stress is lower than the previous disruption case and comparable with the results in Fig. 4. The Fig. 9 reports the Von Mises stresses for this case.

6. RCC-MRx simplified assessment

In spite of the uncertainty related to the load evaluation and their way of application, an A level RCC-MRx criteria was used in this analysis. Fatigue and buckling RCC-MRx criteria were not considered in this analysis. The respect of these criteria prevents from excessive deformation and racheting. This choice has been seemed enough for the kind of approximations really adopted. The RCC MRx provides requirements on materials procurement, design, analysis, construction qualifications, examinations and tests based on feeback from industrial experience. The RCC-MRx code, specific of French nuclear regulation, uses the concept of primary stresses and line supporting segments that are usual for all the nuclear safety assessments. The primary stresses (general membrane P_m and bending P_b) are a linearization of the stresses that equilibrate directly the mechanical applied loads and the line supporting segments are the paths (conveniently defined) along which this linearization is formally executed. The line supporting segments chosen are in the same position reported in [1]. In Fig. 10 these paths have been highlighted in a convenient virtual cut of the solid model.

The related set of analysis has been performed assuming a linear elastic behavior of the material. The first step is to assure that membrane and bending stresses caused by mechanical load (water pressure) at its working temperature are below the allowable stresses at the same temperature. With clear symbolism (θ_m is the mean temperature along the path), in Table 3 there is the

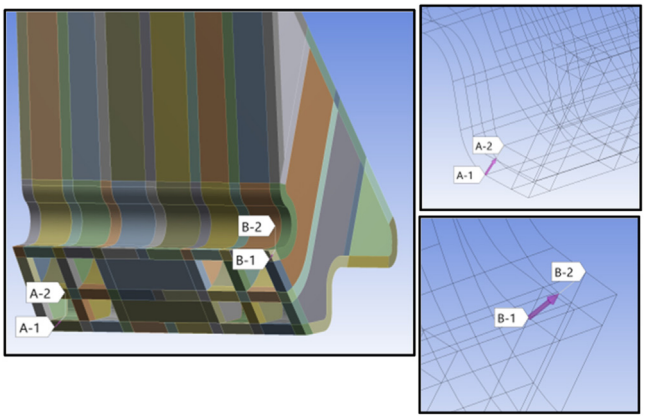

Fig. 10. Path positions for RCC-MRx assessment.

Table 3
Assessment against primary damages.

Path A1–A2	**$\Theta m = 339.34\,^{\circ}C$**
$P_m = 1.64 \cdot 10^6$ Pa	$S_m = 185 \cdot 10^6$ Pa
$P_m + P_b = 2.9 \cdot 10^6$ Pa	$1.5 \cdot S_m = 277 \cdot 10^6$ Pa
Path B1–B2	**$\Theta m = 315.5\,^{\circ}C$**
$P_m = 1.0 \cdot 10^6$ Pa	$S_m = 189 \cdot 10^6$ Pa
$P_m + P_b = 4.33 \cdot 10^6$ Pa	$1.5 \cdot S_m = 284 \cdot 10^6$ Pa

Table 4
Assessment against secondary damages.

Path A1–A2	**$\Theta m = 339.34\,^{\circ}C$**
$Max(Pm + Pb) + \Delta Q = 109 \cdot 10^6$ Pa	$3 \cdot Sm = 555 \cdot 10^6$ Pa
Path B1–B2	**$\Theta m = 315.5\,^{\circ}C$**
$Max(Pm + Pb) + \Delta Q = 238 \cdot 10^6$ Pa	$3 \cdot Sm = 568 \cdot 10^6$ Pa

summary of this point. S_m is reported inside the code as a function of temperature.

The second step has regarded then classical $3S_m$ rule that is the evaluation of the stress range from the stand-by condition (the component at the same temperature of water bulk value) to the maximum thermal stress condition that is with the full action of nuclear heating. With the classical symbolism always used, in the Table 4 the essential results have been reported.

Also in this case as in [1], the simplified assessment has been satisfied.

7. Analysis with cassette shell model

Besides the previous study, another tool has been developed. In order to aid the decision process of the design phase, different *concepts* that potentially meet the design requirements have been investigated in order to choose the "best solution" between more options [10]. In this phase, more than in the others, major changes occur constantly, thus a parametric design approach and the use of lighter finite element models are crucial to speed-up the whole design process, incorporating modifications to the models efficiently [11,12].

Divertor cassette parametric shell model (Fig. 11) has been used to carry out an optimization of the ribs thickness and of the general layout, taking into account coolant pressure, thermal loads and cassette preloading needs. As first stage, comparative analyses with the 3D solid models presented in Section 2 have been performed, applying the same loads and boundary conditions.

In order to prepare future RCC-MRx assessment related to the shell model, both the Von Mises stress (middle) and the top/bottom Von Mises stresses have been obtained. To compare with the 3D

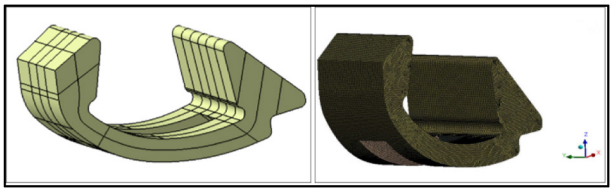

Fig. 11. Parametric Shell model from CATIA V5 to Ansys.

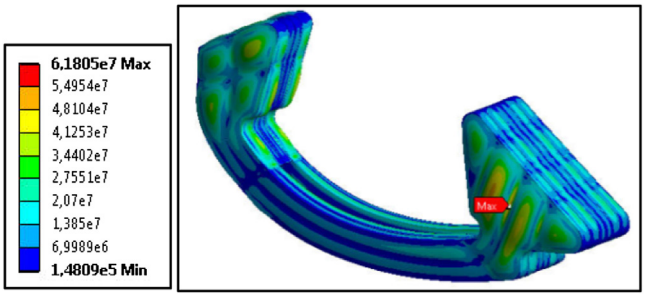

Fig. 12. Von Mises stress for coolant pressure load (top/bottom).

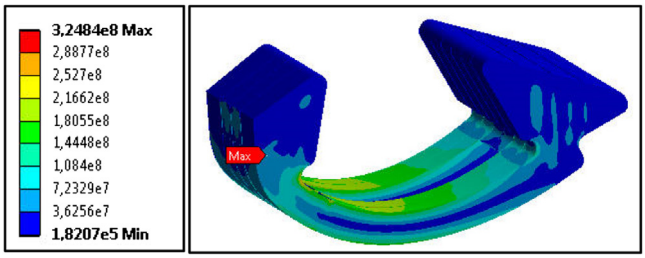

Fig. 13. Von Mises stress for coolant pressure and thermal load (top/bottom).

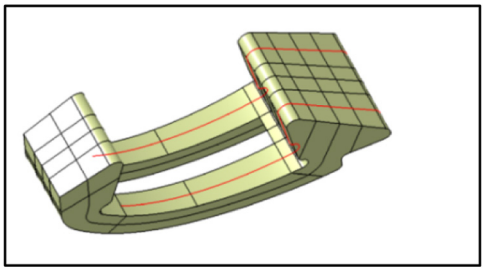

Fig. 14. Poloidal ribs removed.

results shown in Section 2, the top/bottom results for the only coolant pressure and for the combination of coolant pressure and thermal loads are shown respectively in Figs. 12 and 13.

Taking into account the obtained results, a first optimization process has been performed, in terms of ribs layout and thickness. The parametric approach allowed modifications to be implemented efficiently. In particular, the iterative analysis process shows the possibility to remove 2 poloidal ribs (see Fig. 14) and reduce the thickness from 40 mm to 20 mm.

According to first structural analyses, thickness reduction and layout modification are acceptable against pressure and thermal loads as it can be seen in Fig. 15. Furthermore the reduction in the cassette stiffness allows for cassette preloading needed for locking and electrical needs.

Even though the maximum values of equivalent stresses and their positions in the 3D and 2D models are different, the distributions are similar and the order of magnitude agrees well in both cases. So further investigation related to the influence of the

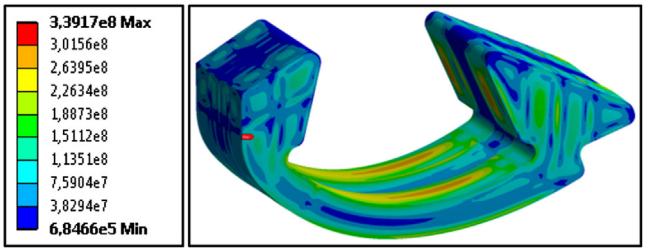

Fig. 15. Equivalent stress for coolant pressure and thermal load (top/bottom) with new ribs configuration.

reduction of the ribs thickness on shielding performances and also their effects on the behaviour of the component against halo currents and EM loads can be carried on.

8. Conclusion

The structural analysis carried out for the reference model of DEMO Divertor cassette body showed that the thermal power to be generated by nuclear heating would give the largest contribution to the final stress state. It was also confirmed that under the normal operation loads, the structural failure criteria are not violated. The final judgment in terms of structural design feasibility can be made once the structural impact of off-normal dynamic loads due to electromagnetic forces (disruptions and vertical displacement events) has been assessed and evaluated against code rules. This work is ongoing.

Acknowledgments

This work has been carried out within the framework of the EUROfusion Consortium and has received funding from the European research and training program 2014–2018 under grant agreement N. 633053. The views and opinions expressed herein do not necessarily reflect those of the European Commission. The computing resources and the related technical support used for this work have been provided by CRESCO/ENEAGRID High Performance Computing infrastructure. It is funded by ENEA, the Italian National Agency for New Technologies, Energy and Sustainable Economic Development and by Italian and European research programs, see http://www.cresco.enea.it/english for information.

References

[1] P. Frosi, G. Mazzone, Structural design of DEMO Divertor Cassette Body: provisional FEM analysis and introductive application of RCC-MRx design rules, Fusion Eng. Des. 109–111 (2016) 47–51.
[2] F. Romanelli, et al., Fusion Electricity – a Roadmap to the Realization of Fusion Energy, European Fusion Development Agreement (EFDA), 2012, ISBN 978–3-00–040720-8.
[3] G. Federici, et al., Overview of EU DEMO design and R&D activities, Fusion Eng. Des. 89 (2014) 882–889.
[4] C. Bachmann, et al., Initial DEMO tokamak design configuration studies, Fusion Eng. Des. 98–99 (2015) 1423–1426.
[5] J.H. You, et al., Conceptual design studies for the European DEMO Divertor. Rationale and first results, Fusion Eng. Des. 109–111 (2016) 1598–1603.
[6] RCC-MRx 2012 AFCEN Edition, Design and Construction Rules for Mechanical Components of Nuclear Installation.
[7] R. Villari, et al., Neutron Analysis Report for Divertor Cassette and PFC, EFDA_D_2MN6FV.
[8] V. Cocilovo, EM Analysis Report for Divertor Cassette Body EFDA_D_2MZGPJ.
[9] M. Roccella, et al., Development of global EM analysis model, EFDA_D_2MMBW.
[10] G. Di Gironimo, et al., Concept design of the DEMO divertor cassette-to-vacuum vessel locking system adopting a systems engineering approach, Fusion Eng. Des. 94 (2015) 72–81.
[11] R. Mozzillo, et al., Development of a master model concept for DEMO vacuum vessel, Fusion Eng. Des. 112 (2016) 497–504.
[12] D. Marzullo, et al., Design progress of the DEMO divertor locking system according to IPADeP methodology, Proced. CIRP 34 (2015) 56–63.